The nervous system is the major target for Gold nanoparticles: Evidence from RNA sequencing data of *C. elegans*

Mo Jihao[1*], Sun Ning[2*], Yang Baolin[3], Li Shaoxia[1], Wang Lei[4,5#]

1 Department of Medical Laboratory, Luoyang Orthopedic Hospital of Henan Province, Orthopedic Institute of Henan Province, Henan, China

2 Institute of Clinical Laboratory Science, Jinling Hospital, School of Medicine, Nanjing University, Nanjing, China.

3 Institute of Technical Biology $ Agriculture Engineering, Hefei Institutes of Physical Science, Chinese Academy of Sciences, Anhui, China

4 School of Biological Sciences, Nanyang Technological University, Singapore

5 Current address: Department of Physiology and Biophysics, Miller School of Medicine, University of Miami, Miami, FL, USA

*These authors contributed equally to this work.

#Author for correspondence (lxw561@miami.edu)

Abstract

The increasing use of gold nanoparticles (NPs) raises concerns about the potential effect of gold NPs exposure on human health. Therefore, gold NPs exposure is hard to evaluate at the organ level with current measurement technology. The bio-distribution assay showed that intestine was the organ with most gold NPs accumulated in *C. elegans*. However, our data indicated that 62.8% of the significant altered genes were function in the nervous system using tissue enrichment analysis. Notably, developmental stage analysis has demonstrated that NP exposure interfered with the development of animals. Furthermore, the transcription factors DAF-16 was regulating the oxidative stress genes induced by gold NPs. Therefore, we proposed the localization of the oxidative stress genes in the neuron cells and how their expression affect neuron communication. Our results demonstrate that the gold NPs-induced oxidative stress affects the nervous system via physical damage to the neurons and disruption of cell-to-cell communication. Future toxicology research on gold NPs should focus on neurons.

Keywords: gold nanoparticles (NPs), nervous system, RNA sequencing, oxidative stress, *C. elegans*.

33 Graphical abstract

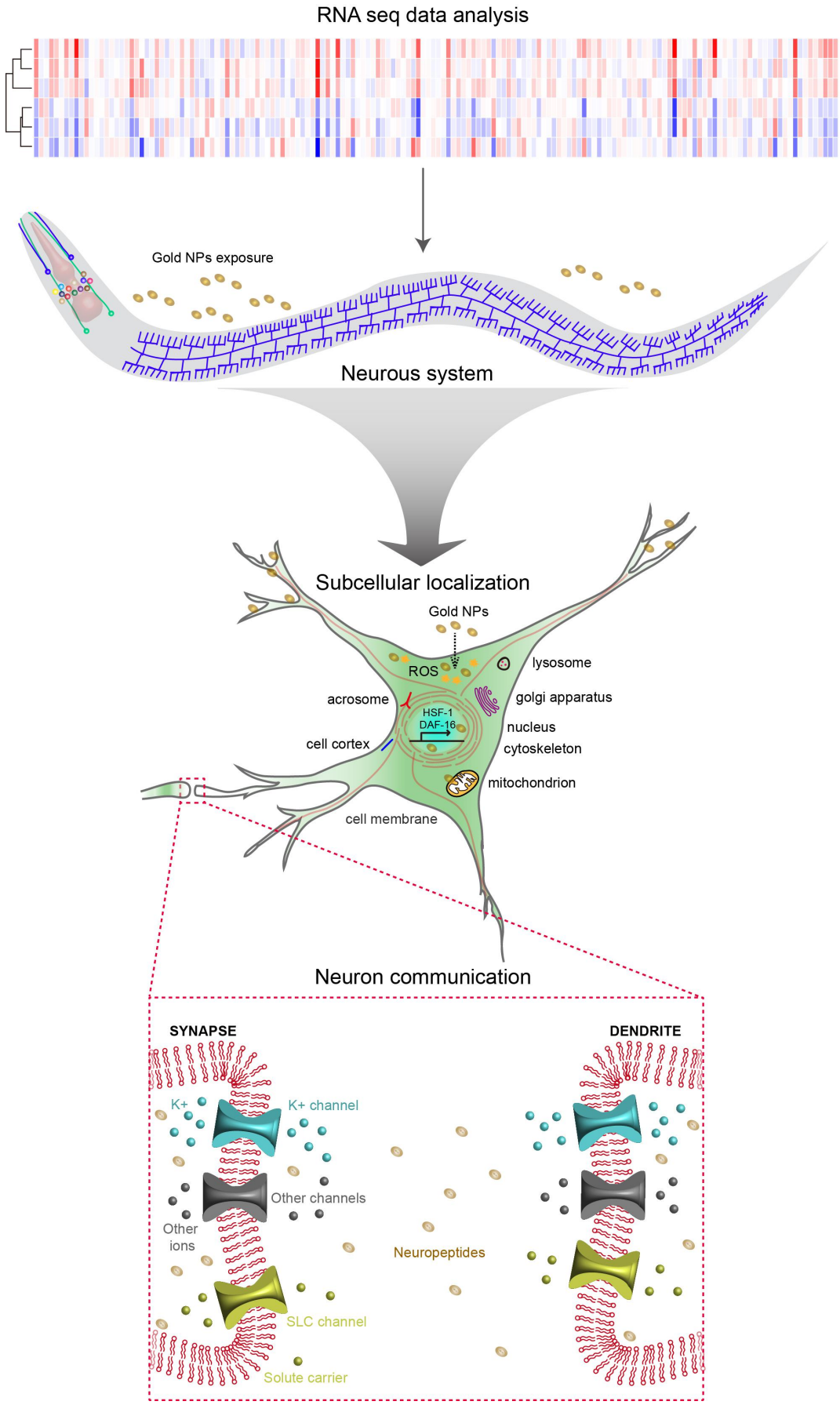

34

35 **Introduction**

36

37 With the development of nanotechnology, there has been growing interest in nano-materials for a wide
38 range of health and medicinal applications. With their nanoscale size, the nano-materials can interact
39 with biological systems at the molecular level to protein, DNA, and RNA [1,2]. Gold NPs, due to the
40 chemical and physical stability, optical property, like stimuli-response surface-enhanced Raman
41 Scattering, surface plasmon resonance in the near infrared region, is one of the most studied
42 nano-materials in bio-medical applications. In recent decades, the interactions between engineered gold
43 NPs and liver, kidney, blood vessels, tumors have been studied [3-6]. Additionally, the gold NPs can
44 partially penetrate the blood-brain barrier in the brain, allowing them to act in the central nervous [7].
45 Targeted drug delivery using gold NPs has been tested on tumors, the liver, lung, and inhalation [8-11].
46 Although relatively low toxicity has been reported on gold NPs, most researchers agree that exposure to
47 nano-scale materials can lead to chronic toxicity, which may be due to the responses at the gene and
48 protein level [12,13].

49

50 Despite the numerous cytotoxicity studies for gold NPs, which have been investigated *in vivo* and *in vitro*,
51 the results vary based on the type of cells used, the time of exposure, the physical and chemical property
52 and the surface modification of the nanomaterials. *In vitro* studies using human oral cancer cell (HSC-3)
53 have demonstrated that gold NPs enter the cytoplasm, mitochondria, and nucleus of the cells. Few
54 publications claim toxicity of gold NPs at a lower concentration than 1 ppm [14]. However, when increased
55 to 10 ppm or higher, increased expression of apoptosis, oxidative stress, and pro-inflammatory genes
56 was reported [15]. Apoptosis, autophagy, DNA damage, and necrosis were also observed in studies in
57 HSC-3, HeLa cells, and liver of BALB/c mice [16-18]. Furthermore, it has been shown that the higher levels

58 of oxidative stress generated by the large surface of gold NPs, which cause DNA and Mitochondrial
59 damage, further disrupts cellular homeostasis [17].
60
61 Biodistribution is a key factor to understand how NPs accumulate and interact with each organ. The
62 current quantification techniques require the isolation of each internal organ or the fluorescent/radio
63 imaging modalities to modulate the whole animal. As well as the biodistribution of the NPs, to understand
64 how each organ responds to NPs *in vivo* is a huge challenge in humans but it is possible in small animals.
65 Studies in mice show that 13 nm PEG-coated gold NPs were mainly deposited in the liver, kuffer cells,
66 and the spleen [19,20]. While other studies in rats proved 18 nm gold NPs were accumulated in the liver and
67 spleen, but 1.4 nm mainly in the kidney [21]. The intestine of *C. elegans*, have the combined function of
68 liver, spleen and kidney, accumulates most of the gold NPs [22]. Although these organs accumulate gold
69 NPs, further investigations should be focused on how each organ responds to the gold NPs, and how the
70 expression of genes in each tissue restore homeostasis.
71
72 *C. elegans* is a transparent animal with multiple important signaling pathways conserved in mammals,
73 like autophagy, insulin, and apoptosis signaling pathways [23]. We analyzed the RNA sequencing data set
74 (GSE32521) from gold NPs exposed worm. However, different with the biodistribution data, the results
75 showed that the nerve system was the most affected when exposing organisms to gold NPs. Further
76 studies show that the oxidative stress transcription factor DAF-16 and HSF-1 are the main transcription
77 factors that regulate the gold NP-induced gene expressions. The ion-channel protein analysis indicated
78 that the potassium and solute carrier (SLC) channels are the most altered channels by gold NPs, which
79 could be the direct way of how gold NPs affect neuron activity.

80

81 **Materials and Methods**

82

83 C. elegans strains and growth conditions

84 The wild type strain (*N2*) and daf-16 reporter strain (*daf-16* (*zls356*)) were gifted from the Caenorhabditis

85 Genetics Center (St. Paul, MN). The synchronized worms were cultured with nematode growth medium

86 plates. The *E.coli* strain *OP50* was used as a food source. All the experiments were performed at 20°C.

87

88 Measurement of Size distribution and zeta potential

89 The 40 nm gold NPs were purchased from Biotech (Jieyi, Shanghai). The gold NPs were originally

90 distributed in water, then diluted in S medium. All the samples were sonicated for 30 minutes before the

91 measurement. The size distribution and zeta potential were tested by a Malvern zeta sizer (HTS3000,

92 Germany). The data was collected and graphed by graphpad 7. The data in the manuscript were labeled

93 as average ± standard deviation.

94

95 Measurement of body length and developmental stage

96 The synchronized wild type nematodes were cultured in NGM plates with 0, 1, 10, 100 mg/L of gold NPs

97 respectively. The *OP50* was added as food resource. The nematodes were observed each day and food

98 was added every 48 hours. Animals were anesthetized by 50 μM sodium azide on slides. The images

99 were taken by Leica microscope with 10X objective lens. The body length was measured by Image J.

100 The developmental stage was determined by observe the phenotype of each organ and the body length.

101 At least 100 worms were counted for each condition. The graph was generated by R. The data in the

102 manuscript were labeled as average ± standard deviation.

103

104 DAF-16 subcellular localization analysis

105 The DAF-16 subcellular localization was used as a reporter to prove the activation of insulin like receptor

106 pathway. The *daf-16p::daf-16a/b::GFP* allele nematodes were cultured to L4 stage and then transferred

107 to the 60 mm petri dishes with 0, 100 mg/L gold NPs respectively. After 24 hours, the worms were

108 mounted on slides with sodium azide for imaging. The worms of positive control group were exposed to

109 37°C for 1 hour. The images were taken by Leica fluorescence microscope with a 20X objective lens. The

110 number of cells with clear nucleus localization was counted and plotted by graphpad 7. The data in the

111 graph was labeled as average ± standard error.

112

113 Quantitative Realtime-PCR

114 The wildtype nematodes were cultured to L4 stage and then transferred to the 60 mm petri dishes with 0,

115 100 mg/L gold NPs respectively. The RNA of each sample was extracted by TRIZOL (Thermo Fisher,

116 Waltham, MA) as described [24]. The contaminant DNA was removed by TURBO DNase (Thermo Fisher).

117 The complementary DNA was synthesized from total RNA using Reverse transciptase (Thermo Fisher).

118 QPCR was performed with SYBR Green using a Bio-Rad CFX-96 (Hercules, CA, USA) real-time PCR

119 system. Thirty ng of cDNA was used as templet and 50 nM of paired primer mix of each gene were used

120 for each reaction. Relative mRNA expression of the target genes was normalized to *act-1*. The primers

121 used in this manuscript were listed below. The individual experiment was repeated at least three times.

122 The data in the graph was labeled as average ± standard error.

123

gene	Forward	Reverse
acly-1	GCCCTGGAAGTGTCGCCTAT	CAGGTTCCGATGCACCATGC
act-1	CCAGAGCGCAAGTACTCCGT	AGCTGGTGGTGACGATGGTTT
cpr-5	CGCTACTGAGGTCTCCGACG	AGGATCCTCCGGTGACGAGA
lpr-3	AACCAATTGCCCTCCCACCA	GTACGGCTCCAGCGAATCCT
mex-5	CGCCGACCAAAGTGATGCTC	CGACGCTTGTTCATCGGTGG
nkcc-1	CGGGGTAGTTGCCGAAGTGT	ACGCCCAACTCGACATCATC
sop-2	CACATGTGGCCCGAATCACG	TCGCGTCGTTATCCACCTCC

124

125 RNA sequencing data Analysis

126 The RNA sequencing data, reference series GSE32521, was obtained from Gene Expression Omnibus,

127 National Center for Biotechnology Information. Age-synchronized L3 worms were exposed to 4 nm gold

128 NPs with a concentration of 5.9 mg/L in 50% K-Medium. Then they were cultured with 50% K-Medium

129 and left for another 12h. The RNA was extracted from each of the replicates. Significantly changed genes

130 with 1.5 fold and $p < 0.05$ and FDR < 0.1 were analyzed [22].

131

132 Gene Expression Analysis

133 The volcano plot was generated by R (version 3.5.2) using package ggplot2. Significantly changed genes

134 with 1.5 fold and $p < 0.05$ were marked red. Genes with 1.5 fold and $p > 0.05$ were marked blue. The

135 tissue enrichment analysis was proceeded by Gene Set Enrichment Analysis function of Wormbase

136 (https://www.wormbase.org/tools/enrichment/tea/tea.cgi) [25]. The color of each sub-tissue was marked

137 based on the tissue. The motif sequence was analyzed using the motif discovery function of MEME

138 (http://meme-suite.org/tools/meme) [26]. The length of the enriched motifs was set between 6 to 50

139 nucleotides.

140

141 Protein function and sub-cellular localization analysis

142 The protein-protein function analysis was measured using genes that significantly increased in
143 expression. The co-expression, genetic interactions and physical interactions were used as parameters
144 to analyze the interaction using Genemania (https://genemania.org/) [27]. The top 20 genes with increased
145 expression were marked by differences in function using STRING
146 (https://string-db.org/cgi/input.pl?sessionId=pSsnm1zTtNsB&input_page_show_search=on) [28]. The
147 sub-cellular localization analysis was investigated based on the structure domain and signal sequence
148 using iLoc-Animal (http://www.jci-bioinfo.cn/iLoc-Animal) [29]. The number of enriched proteins in each
149 organelle was shown by using a heat map.

150

151 Ion Channel protein Analysis

152 The proteins specific to each ion channel were isolated from RNA sequencing data as previously
153 reported [30]. The genes significantly changed in expression, were analyzed and data was shown using a
154 heat map generated by R. The activation of each ion channel was predicted based on the change in
155 expression of ion channel proteins.

156

157 **Results**

158 The nervous system is the most affected by gold NPs

159 In mice, the liver and spleen are the target organs for gold NPs accumulation [21]. In *C. elegans*, the
160 intestine plays a role as the liver, kidney, spleen, and stomach, which is also the organ that has most gold
161 NPs accumulated [22]. For the worms treated with 4 nm gold NPs, 773 genes were significantly increased
162 for at least 2-fold and 268 genes were significantly decreased for at least 2-fold (Fig. 1A). The tissue

163 enrichment assay showed that 62.8% of the significantly altered genes are localized in neuron cells,
164 14.9% enriched intestine, 7.8% for reproductive system, 1.6% for muscles and 13% for other tissues (Fig.
165 1B). The PVD neuron and outer labial sensillum have genes significantly increased and decreased, while
166 the thermosensory neuron, amphid sensillum, pharyngeal interneuron, ASE, lateral ganglion, touch
167 receptor neuron, BDU and retrovesicular ganglion have genes only significantly increased, nerve ring
168 and lateral, dorsal nerve cord have genes only significantly decreased (Fig. 1C). The intestine enriched
169 genes show a significant increase only. Meanwhile, the reproductive system and muscle enriched genes
170 shows a significant decrease. From the analysis of the promoter sequence of all the significantly
171 increased genes, a conserved 43 base pairs motif with an e value of 1.5^{-222} was found. This result
172 indicates that the nervous system is the most affected organ by gold NPs exposure and most of the
173 significantly increased genes are enriched in the nervous system and intestine. Most of the significantly
174 decreased genes are enriched in the reproductive system and muscle. To further understand how gold
175 NPs interact with the nervous system, the significantly increased genes which enriched in the nervous
176 system were analyzed by protein-protein interaction assays. In all the significantly increased genes, 20 of
177 them showed more interaction with other proteins (Fig. 1E). Function analysis showed that they are
178 involved in cellular component organization (*let-2, dyn-1, unc-51, unc-54, chc-1, ama-1, sec-24.2, eif-3.B,*
179 *tfg-1,* and *F13B9.1*), reproduction *(let-1, dyn-1, snx-14, unc-54, H28O16.1, dlst-1, chc-1, copb-1, csnk-1,*
180 *eif-3.B, ama-1, tsr-1, sec-24.2,* and *tfg-1*), multicellular organismal development (*let-1, dyn-1, T22F3.3,*
181 *unc-54, H28O16.1, dlst-1, chc-1, csnk-1, eif-3.B, ama-1, tsr-1, sec-24.2, pme-5,* and *tfg-1*) , nematode
182 larval development (*let-2, dyn-1, unc-51, T22F3.3, unc-54, H28O16.1, dlst-1, chc-1, csnk-1, eif-3.B,*
183 *ama-1, sec-24.2,* and *tfg-1*) and embryo development in birth or egg hatching (*let-1, dyn-1, T22F3.3,*
184 *H28O16.1, dlst-1, chc-1, csnk-1, eif-3.B, ama-1, tsr-1, sec-24.2*, pme-5 and *tfg-1*) (Fig. 1F).

185

186 Gold NPs regulate development and reproduction through the nervous system

187 To investigate how gold NPs interact with *C. elegans* in the culture environment, the size distribution and
188 zeta potential were measured in water and S medium. With the increase of concentration, the real size of
189 gold NPs increased (Fig.2A&2B). The average hydrodynamic diameter of 1, 10, 100 mg/L gold NPs in S
190 medium are 94.4 ± 29.9, 952.4 ± 150.1, and 1144.3 ± 159.7 nm, respectively. There was no significant
191 difference between the zeta potential of gold NPs in water and in S medium. The zeta potential for S
192 medium are -5.93, -14.6, and -6.6 mV respectively (Fig.2C&2D). These results indicated that gold NPs
193 have a larger size in S medium than water, but the dispersion is very stable after sonication. To further
194 understand how gold NPs affect the function of the nervous system, gene ontology analysis was
195 proceeded by the list of nervous system enriched genes. From the 32 significantly enriched terms, 10 of
196 them were related to development, including larval, embryo, genitalia, multicellular organism, vulval,
197 gonad, germ cell, and dendrite development. Several cell signaling pathways were shown to be affected,
198 as endocytosis, apoptosis, phosphorylation, cell differentiation, secretion. There are also some
199 phenotype related changes as reproduction, locomotion, morphogenesis, oviposition, lifespan,
200 oogenesis and oocyte maturation (Fig. 2E). These results indicated that Gold NPs exposure regulates
201 development and reproduction through the nervous system. To further confirm the effect of gold NPs on
202 the development of *C. elegans*, the developmental assay was preformed by start exposure from L1 stage.
203 As shown in Fig.2F and 2G, expose to 10, 100 mg/L of gold NPs significantly affected the development of
204 *C. elegans.* The body length of control, 1, 10, 100 mg/L gold NPs are 1068.2 ± 95.3, 1086.6 ± 108.3,
205 1028.2 ± 155.8, and 771 ± 86.9 μm respectively. After 60 hours of culture, the wildtype control group
206 have 41.4%of worm developed to adult, 55.2% of worm as young adult, 3% as L4 stage. The 1 mg/L gold

207 NPs have 44.1% adult, 50.4% as young adult, 5.5% as L4 stage. For the 10 mg/L exposure group, 44.0%
208 adult, 26.7% as young adult, 29.3% as L4 stage. For the 100 mg/L exposure group, 0.8% young adult,
209 92.3% as L4 stage, 6.8% as L3 stage (Fig.2H). These results indicate that the 10 and 100 mg/L gold NPs
210 delayed the development of *C. elegans* in a concentration dependent manner.
211
212 Gold NPs damage the nervous system mainly through oxidative stress.
213 Since the nervous system was the most affected organ by gold NPs exposure, we further investigated
214 the mechanism of how gold NPs affect the nervous system function. Oxidative stress has been reported
215 as the main factor causes damage when the cells and mice were exposed to gold NPs [17,19]. We analyzed
216 our data by comparing the reactive oxygen species signaling in *C. elegans* dataset (GSE54024) [31]. From
217 all the genes significantly increased and enriched in the nervous system, 26.5% of them were related to
218 reactive oxygen species signaling pathway (Fig. 3A). Gene ontology showed these 62 genes were
219 related to development, reproduction endocytosis, locomotion and egg hatching (data not shown). In *C.*
220 *elegans*, the transcription starts from the transcription factor binding site by recognizing specific DNA
221 motif. DAF-16 is one of the most well-known oxidative stress regulation transcription factors in *C. elegans*
222 [32]. The motif in the promoter region that DAF-16 binds to have been well established. From the DNA
223 sequence analysis near the promoter region, 59 out of 62 genes contain DAF-16 binding motif. The
224 binding motif in the promoter region of *unc-11, nep-17* and *acs-13* have been graphed (Fig. 3B). To
225 further confirm the activation of insulin-like receptor pathway, *daf-16p::daf-16a/b::GFP* mutant was used.
226 As shown in Fig.3C&D, the worms from 100 mg/L gold NPs exposure group have obverse nucleus
227 localization compare to control worms. The average number of control, 100 mg/L gold NPs, and heat
228 shock group for DAF-16 nucleus localized cells are 10.2 ± 4.5, 48.3 ± 10.7, 164.0 ± 8.6, respectively. To

229 confirm the daf-16 regulated oxidative stress respond genes were activated by gold NPs exposure, we
230 preformed the real time PCR analysis. The enriched genes as *cpr-5, sop-2*, and *acly-1* are not
231 significantly changed in mRNA expression. While genes as *nkcc-1, lpr-3,* and *mex-5* are significantly
232 increased in mRNA expression. The difference in the RNA-seq enriched target genes and our real time
233 PCR results might due to the difference in worm culture medium, and the size and synthesis method of
234 gold NPs. This result indicates that the nervous system regulates gold NPs exposure induced oxidative
235 stress mainly through transcription factor DAF-16. The oxidative stress downstream gene *nkcc-1, lpr-3*,
236 and *mex-5* are the target genes for gold NPs exposure.
237
238 Gold NPs enriched oxidative stress genes are mainly expressed in the cytoplasm and nucleus in neuron
239 cells.
240 Since oxidative stress is the main way for gold NPs to damage neuron cells, we further analyzed the
241 subcellular distribution of the significantly increased and nervous system enriched genes that related to
242 the reactive oxygen species signaling pathway. From the protein sequence based subcellular localization
243 prediction, 57 out of 62 genes have been localized to each specific organelle. Forty genes were predicted
244 to be localized in the cytoplasm, 23 in the nucleus and 3 in the mitochondrion (Fig.4A and 4B). Neuron
245 cells communicate with each other by using signal molecules to send and receive ions and transporters.
246 Therefore, changes in ion channel proteins, transporters, receptors, motor proteins and complexes have
247 a huge impact on the stress response, movement and energy metabolism of the organism. Hereby, we
248 analyzed the ion channel genes that significantly changed in expression when worm exposed to gold
249 NPs. The *twk-47* from K+ channel, *ncx-2* and *nkcc-1* from SLC channel, *nep-17* and *nep-18* from
250 neuropeptides metabolism. The *egl-30, gpb-1* and *snx-14* from downstream of GPCRs, the *dlg-1, afd-1*

251 and *shn-1* from PDZ domain proteins, the *klp-7* and *klp-10* from kinesin-like motor proteins, the *hum-7*
252 from myosin motors, the *unc-52* and *mig-6* from extracellular immunoglobulin and leucine-rich repeat
253 domain-containing proteins and the *hmr-1* from cadherins were significantly increased in *C. elegans*
254 exposed to gold NPs. This result indicates that the proteins affected by gold NPs exposure were mostly
255 located in the cytoplasm and nucleus. The communication of neuron cells might be affected through
256 several significantly changed channel proteins and neuron transmitter proteins.
257
258 **Discussion**
259 Considering the growing interest in gold NPs used in nanomedicine and target drug delivery, the potential
260 health effect of gold NPs need to be well studied. A lot of research has been done to investigate the effect
261 of gold NPs on cancers, the lung and neuron cells [4,16,33]. More detail needs to be investigated at the
262 organ level. Although biodistribution assays have been done on *C. elegans* and mice [22,34], the organ
263 (intestine for worm, liver, kuffer cells and spleen for mice) have most gold NPs accumulated, has a
264 higher possibility to be the organ damaged. However, based on the analysis of whole-body RNA-seq
265 data from *C. elegans,* our research shows the nervous system was most affected.
266
267 Many researchers have demonstrated that gold NPs exhibit less cytotoxic and genotoxic effects
268 compared to other nanomaterials like Zn and Ag NPs [35,36]. However, research in *Drosophila*
269 *melanogaster* reported the gold NPs induces decreased infertility and numbers of progeny, increased in
270 aberrant phenotype [37]. These results indicating that gold NPs might affect the development of animals,
271 mostly in the reproductive system. Similar research conducted in *C. elegans* claimed that gold NPs
272 maternal exposure causes a trans-generational effect [38]. Furthermore, gold NPs disrupt eye development

273 and pigmentation in Zebrafish [39]. Our finding claimed that most of the nervous system enriched genes,
274 which significantly changed in expression in gold NPs exposed worms, are development related genes.
275 Data from developmental stage analysis also confirmed our finding. Future studies will investigate how
276 neurons regulate development when exposing to gold NPs.
277
278 Many cellular responses induced by gold NPs, such as unfolded protein stress, apoptosis and DNA
279 damage, are characterized by an increase in the oxidative stress. Previous experiments demonstrated
280 that 1.4 nm gold NPs induce necrosis in HeLa cells by oxidative stress further amplified by mitochondrial
281 damage [17]. Gold NPs induced apoptosis and upregulation of pro-inflammatory genes were discovered [15].
282 The researcher claimed that smaller Au NPs with larger surface area, might yield higher levels of
283 oxidative stress. Gold NPs with a diameter less than 50 nm can easily penetrate the cell membranes and
284 enter the nucleus of the cells [33,40-42]. In our data, 40 nm gold NPs significantly increased the mRNA
285 expression of several *daf-16* regulated oxidative stress genes, which showed how the neurons response
286 to the oxidative stress.
287
288 Gold NPs modulate neural activity has been studied in multiple nervous systems [43,44]. It has been shown
289 that gold NPs increase neurite length, promoter adhesion and proliferation, change the action potentials,
290 and affect Ca^{2+} influx [45-47]. Furthermore, engineered gold NPs were able to bind to sodium channels,
291 transient receptor potential vanilloid member 1 channels, and P2X3 receptor ion channel in dorsal root
292 ganglion neurons, which affect the neuron-neuron communication [44]. Our data showed that genes related
293 to potassium channel, SLC channel, GPCR, cadherins, motor proteins were upregulated by gold NPs

exposure, which indicated that gold NPs might affected the function of related channels. Further research should be conducted on how related channels regulates the ions further affect neuron communication.

Acknowledgement

We are grateful to our colleagues Cristina Johnson Kay and Nicole Encalada for critical reading of the manuscript.

300 **References**

301 1 Weissleder, R., Kelly, K., Sun, E. Y., Shtatland, T. & Josephson, L. Cell-specific targeting of
302 nanoparticles by multivalent attachment of small molecules. *Nature biotechnology* **23**,
303 1418-1423, doi:10.1038/nbt1159 (2005).

304 2 Saptarshi, S. R., Duschl, A. & Lopata, A. L. Interaction of nanoparticles with proteins: relation
305 to bio-reactivity of the nanoparticle. *Journal of nanobiotechnology* **11**, 26,
306 doi:10.1186/1477-3155-11-26 (2013).

307 3 Dragoni, S. *et al.* Gold nanoparticles uptake and cytotoxicity assessed on rat liver
308 precision-cut slices. *Toxicological sciences : an official journal of the Society of Toxicology* **128**,
309 186-197, doi:10.1093/toxsci/kfs150 (2012).

310 4 Zhao, M. X., Cai, Z. C., Zhu, B. J. & Zhang, Z. Q. The Apoptosis Effect on Liver Cancer Cells of
311 Gold Nanoparticles Modified with Lithocholic Acid. *Nanoscale research letters* **13**, 304,
312 doi:10.1186/s11671-018-2653-8 (2018).

313 5 Sereemaspun, A., Rojanathanes, R. & Wiwanitkit, V. Effect of gold nanoparticle on renal cell:
314 an implication for exposure risk. *Renal failure* **30**, 323-325, doi:10.1080/08860220701860914
315 (2008).

316 6 Nethi, S. K. *et al.* Bioconjugated gold nanoparticles accelerate the growth of new blood
317 vessels through redox signaling. *Chem Commun* **50**, 14367-14370, doi:10.1039/c4cc06996j
318 (2014).

319 7 Cheng, Y. *et al.* Blood-brain barrier permeable gold nanoparticles: an efficient delivery
320 platform for enhanced malignant glioma therapy and imaging. *Small* **10**, 5137-5150,
321 doi:10.1002/smll.201400654 (2014).

322 8 Kreyling, W. G. *et al.* Age-Dependent Rat Lung Deposition Patterns of Inhaled 20 Manometer
323 Gold Nanoparticles and their Quantitative Biokinetics in Adult Rats. *Acs Nano* **12**, 7771-7790,
324 doi:10.1021/acsnano.8b01826 (2018).
325 9 Dixit, S. *et al.* Transferrin receptor-targeted theranostic gold nanoparticles for photosensitizer
326 delivery in brain tumors. *Nanoscale* **7**, 1782-1790, doi:10.1039/c4nr04853a (2015).
327 10 Kim, B. *et al.* Tuning payload delivery in tumour cylindroids using gold nanoparticles. *Nat*
328 *Nanotechnol* **5**, 465-472, doi:10.1038/Nnano.2010.58 (2010).
329 11 Morshed, R. A. *et al.* Cell-Penetrating Peptide-Modified Gold Nanoparticles for the Delivery of
330 Doxorubicin to Brain Metastatic Breast Cancer. *Mol Pharm* **13**, 1843-1854,
331 doi:10.1021/acs.molpharmaceut.6b00004 (2016).
332 12 Botha, T. L., Boodhia, K. & Wepener, V. Adsorption, uptake and distribution of gold
333 nanoparticles in Daphnia magna following long term exposure. *Aquat Toxicol* **170**, 104-111,
334 doi:10.1016/j.aquatox.2015.11.022 (2016).
335 13 Pacheco, A., Martins, A. & Guilhermino, L. Toxicological interactions induced by chronic
336 exposure to gold nanoparticles and microplastics mixtures in Daphnia magna. *The Science of*
337 *the total environment* **628-629**, 474-483, doi:10.1016/j.scitotenv.2018.02.081 (2018).
338 14 Das, M., Shim, K. H., An, S. S. A. & Yi, D. K. Review on gold nanoparticles and their
339 applications. *Toxicology and Environmental Health Sciences* **3**, 193-205,
340 doi:10.1007/s13530-011-0109-y (2011).
341 15 Yen, H. J., Hsu, S. H. & Tsai, C. L. Cytotoxicity and immunological response of gold and silver
342 nanoparticles of different sizes. *Small* **5**, 1553-1561, doi:10.1002/smll.200900126 (2009).
343 16 Kang, B., Mackey, M. A. & El-Sayed, M. A. Nuclear Targeting of Gold Nanoparticles in Cancer

344 Cells Induces DNA Damage, Causing Cytokinesis Arrest and Apoptosis. *J Am Chem Soc* **132**,
345 1517-+, doi:10.1021/ja9102698 (2010).
346 17 Pan, Y. *et al.* Gold nanoparticles of diameter 1.4 nm trigger necrosis by oxidative stress and
347 mitochondrial damage. *Small* **5**, 2067-2076, doi:10.1002/smll.200900466 (2009).
348 18 Li, J. J., Hartono, D., Ong, C. N., Bay, B. H. & Yung, L. Y. L. Autophagy and oxidative stress
349 associated with gold nanoparticles. *Biomaterials* **31**, 5996-6003,
350 doi:10.1016/j.biomaterials.2010.04.014 (2010).
351 19 Cho, W. S. *et al.* Acute toxicity and pharmacokinetics of 13 nm-sized PEG-coated gold
352 nanoparticles. *Toxicology and applied pharmacology* **236**, 16-24,
353 doi:10.1016/j.taap.2008.12.023 (2009).
354 20 Li, X. *et al.* The systematic evaluation of size-dependent toxicity and multi-time
355 biodistribution of gold nanoparticles. *Colloids Surf B Biointerfaces* **167**, 260-266,
356 doi:10.1016/j.colsurfb.2018.04.005 (2018).
357 21 Semmler-Behnke, M. *et al.* Biodistribution of 1.4- and 18-nm gold particles in rats. *Small* **4**,
358 2108-2111, doi:10.1002/smll.200800922 (2008).
359 22 Tsyusko, O. V. *et al.* Toxicogenomic Responses of the Model Organism Caenorhabditis elegans
360 to Gold Nanoparticles. *Environ Sci Technol* **46**, 4115-4124, doi:10.1021/es2033108 (2012).
361 23 Leung, M. C. *et al.* Caenorhabditis elegans: an emerging model in biomedical and
362 environmental toxicology. *Toxicological sciences : an official journal of the Society of*
363 *Toxicology* **106**, 5-28, doi:10.1093/toxsci/kfn121 (2008).
364 24 Lei, W., Beaudoin-Chabot, C. & Thibault, G. Glucose increases the lifespan of
365 post-reproductive C. elegans independently of FOXO. 347435,

366 doi:10.1101/347435 %J bioRxiv (2018).

367 25 Angeles-Albores, D., RY, N. L., Chan, J. & Sternberg, P. W. Tissue enrichment analysis for C.
368 elegans genomics. *BMC bioinformatics* **17**, 366, doi:10.1186/s12859-016-1229-9 (2016).

369 26 Bailey, T. L. & Noble, W. S. Searching for statistically significant regulatory modules.
370 *Bioinformatics* **19 Suppl 2**, ii16-25, doi:10.1093/bioinformatics/btg1054 (2003).

371 27 Warde-Farley, D. *et al.* The GeneMANIA prediction server: biological network integration for
372 gene prioritization and predicting gene function. *Nucleic acids research* **38**, W214-220,
373 doi:10.1093/nar/gkq537 (2010).

374 28 Szklarczyk, D. *et al.* STRING v11: protein-protein association networks with increased
375 coverage, supporting functional discovery in genome-wide experimental datasets. *Nucleic*
376 *acids research* **47**, D607-D613, doi:10.1093/nar/gky1131 (2019).

377 29 Lin, W. Z., Fang, J. A., Xiao, X. & Chou, K. C. iLoc-Animal: a multi-label learning classifier for
378 predicting subcellular localization of animal proteins. *Molecular bioSystems* **9**, 634-644,
379 doi:10.1039/c3mb25466f (2013).

380 30 Hobert, O. The neuronal genome of Caenorhabditis elegans. *WormBook : the online review of*
381 *C. elegans biology*, 1-106, doi:10.1895/wormbook.1.161.1 (2013).

382 31 Yee, C., Yang, W. & Hekimi, S. The Intrinsic Apoptosis Pathway Mediates the Pro-Longevity
383 Response to Mitochondrial ROS in C. elegans. *Cell* **157**, 897-909,
384 doi:10.1016/j.cell.2014.02.055 (2014).

385 32 Chavez, V., Mohri-Shiomi, A., Maadani, A., Vega, L. A. & Garsin, D. A. Oxidative stress enzymes
386 are required for DAF-16-mediated immunity due to generation of reactive oxygen species by
387 Caenorhabditis elegans. *Genetics* **176**, 1567-1577, doi:10.1534/genetics.107.072587 (2007).

388 33 Jung, S. *et al.* Intracellular gold nanoparticles increase neuronal excitability and aggravate
389 seizure activity in the mouse brain. *PLoS One* **9**, e91360, doi:10.1371/journal.pone.0091360
390 (2014).
391 34 Ibrahim, K. E., Al-Mutary, M. G., Bakhiet, A. O. & Khan, H. A. Histopathology of the Liver,
392 Kidney, and Spleen of Mice Exposed to Gold Nanoparticles. *Molecules* **23**, doi:Artn 1848
393 10.3390/Molecules23081848 (2018).
394 35 Parveen, A. & Rao, S. Cytotoxicity and Genotoxicity of Biosynthesized Gold and Silver
395 Nanoparticles on Human Cancer Cell Lines. *J Clust Sci* **26**, 775-788,
396 doi:10.1007/s10876-014-0744-y (2015).
397 36 Pati, R., Das, I., Mehta, R. K., Sahu, R. & Sonawane, A. Zinc-Oxide Nanoparticles Exhibit
398 Genotoxic, Clastogenic, Cytotoxic and Actin Depolymerization Effects by Inducing Oxidative
399 Stress Responses in Macrophages and Adult Mice. *Toxicological sciences : an official journal*
400 *of the Society of Toxicology* **150**, 454-472, doi:10.1093/toxsci/kfw010 (2016).
401 37 Pompa, P. P. *et al.* In Vivo toxicity assessment of gold nanoparticles in Drosophila
402 melanogaster. *Nano Research* **4**, 405-413, doi:10.1007/s12274-011-0095-z (2011).
403 38 Kim, S. W., Kwak, J. I. & An, Y. J. Multigenerational study of gold nanoparticles in
404 Caenorhabditis elegans: transgenerational effect of maternal exposure. *Environmental*
405 *science & technology* **47**, 5393-5399, doi:10.1021/es304511z (2013).
406 39 Kim, K. T., Zaikova, T., Hutchison, J. E. & Tanguay, R. L. Gold Nanoparticles Disrupt Zebrafish
407 Eye Development and Pigmentation. *Toxicological Sciences* **133**, 275-288,
408 doi:10.1093/toxsci/kft081 (2013).
409 40 Chithrani, B. D., Stewart, J., Allen, C. & Jaffray, D. A. Intracellular uptake, transport, and

410 processing of nanostructures in cancer cells. *Nanomedicine : nanotechnology, biology, and*
411 *medicine* **5**, 118-127 (2009).
412 41 Chithrani, D. B., Dunne, M., Stewart, J., Allen, C. & Jaffray, D. A. Cellular uptake and transport
413 of gold nanoparticles incorporated in a liposomal carrier. *Nanomedicine : nanotechnology,*
414 *biology, and medicine* **6**, 161-169, doi:10.1016/j.nano.2009.04.009 (2010).
415 42 Nativo, P., Prior, I. A. & Brust, M. Uptake and intracellular fate of surface-modified gold
416 nanoparticles. *Acs Nano* **2**, 1639-1644, doi:10.1021/nn800330a (2008).
417 43 Papastefanaki, F. *et al.* Intraspinal Delivery of Polyethylene Glycol-coated Gold Nanoparticles
418 Promotes Functional Recovery After Spinal Cord Injury. *Mol Ther* **23**, 993-1002,
419 doi:10.1038/mt.2015.50 (2015).
420 44 Lin, Y. L., Jen, J. C., Hsu, S. H. & Chiu, I. M. Sciatic nerve repair by microgrooved nerve conduits
421 made of chitosan-gold nanocomposites. *Surg Neurol* **70**, 9-18,
422 doi:10.1016/j.surneu.2008.01.057 (2008).
423 45 Bhang, S. H. *et al.* pH-triggered release of manganese from MnAu nanoparticles that enables
424 cellular neuronal differentiation without cellular toxicity. *Biomaterials* **55**, 33-43,
425 doi:10.1016/j.biomaterials.2015.03.025 (2015).
426 46 Carvalho-de-Souza, J. L. *et al.* Photosensitivity of neurons enabled by cell-targeted gold
427 nanoparticles. *Neuron* **86**, 207-217, doi:10.1016/j.neuron.2015.02.033 (2015).
428 47 Das, S. *et al.* In vivo studies of silk based gold nano-composite conduits for functional
429 peripheral nerve regeneration. *Biomaterials* **62**, 66-75,
430 doi:10.1016/j.biomaterials.2015.04.047 (2015).
431

432 **Figure Legends**

433

434 Figure 1. The nervous system is the most affected organ in *C. elegans* after gold NPs exposure. (A)
435 Volcano plot depicting changes in gene expression in *C. elegans* after gold NPs exposure was analyzed.
436 Gene fold changes are plotted against a *P* value. Genes with upregulated or downregulated by more than
437 1.5 fold and with a FDR less than 0.05 are marked as blue circles. Genes with upregulated or
438 downregulated by less than 1.5 fold and with a FDR more than 0.05 are marked as red circles. (B) Pie
439 graph and (C) bar graph of the tissue enrichment analysis of genes upregulated (blue) and
440 downregulated (red) in gold NPs exposed *C. elegans* group. (D) DNA motif sequence enriched in the
441 promoter region of genes upregulated in *C. elegans* after gold NPs exposure. (E) The protein-protein
442 interaction map of genes upregulated in the gold NPs exposed C. elegans group. (F) The protein-protein
443 interaction between the top 20 upregulated genes. The biological process of each gene was marked
444 based on gene functions.

445

446 Figure 2. The developmental stage analysis of the gold NPs exposed C. elegans group. The size
447 distribution of 40 nm gold NPs in water (A) and S medium (B). The zeta potential of 40 nm gold NPs in
448 water (C) and S medium (D). (E) Bar graph of the biological process analysis of genes upregulated in the
449 gold NPs exposed *C. elegans* group based on *P* value. The development related biological process was
450 marked as blue, others was marked as yellow. (F) The images of L1 worm exposed to 0, 1, 10, 100 mg/L
451 gold NPs after 60 hours. (G) The quantification of (F). (H) The developmental stage analysis of L1 worm
452 exposed to 0, 1, 10, 100 mg/L gold NPs after 60 hours.

453

454 Figure 3. The gold NPs induced oxidative stress in the nervous system were regulated through
455 transcription factor DAF-16. (A) Venn diagram of genes enriched in oxidative stress induced by treatment
456 with the pro-oxidant paraquat and genes enriched in nervous system induced by gold NPs. (B) The
457 location of DNA motif recognized by transcription factor DAF-16 in the promoter region of *unc-11*, *nep-17*
458 and *acs-13*. (C) The image of daf-16 subcellular localization for control, 100 mg/L gold NPs and heat
459 shock groups. (D) The quantification of (C). (E-J) The mRNA expression of *cpr-5, nkcc-1, sop-2, acly-1,*
460 *lpr-3,* and *mex-5* for control and 100 mg/L gold NPs exposure group.
461
462 Figure 4. The gold NPs induced oxidative stress affects multiple organelles in neuron cells and their
463 communication. (A) The heat map and (B) the schematic diagram of subcellular location of the oxidative
464 stress genes enriched in neuron cells. (C) The heat map and (B) the schematic diagram of the oxidative
465 stress affected channel genes which functions in neuron cell communication.

Figure 1

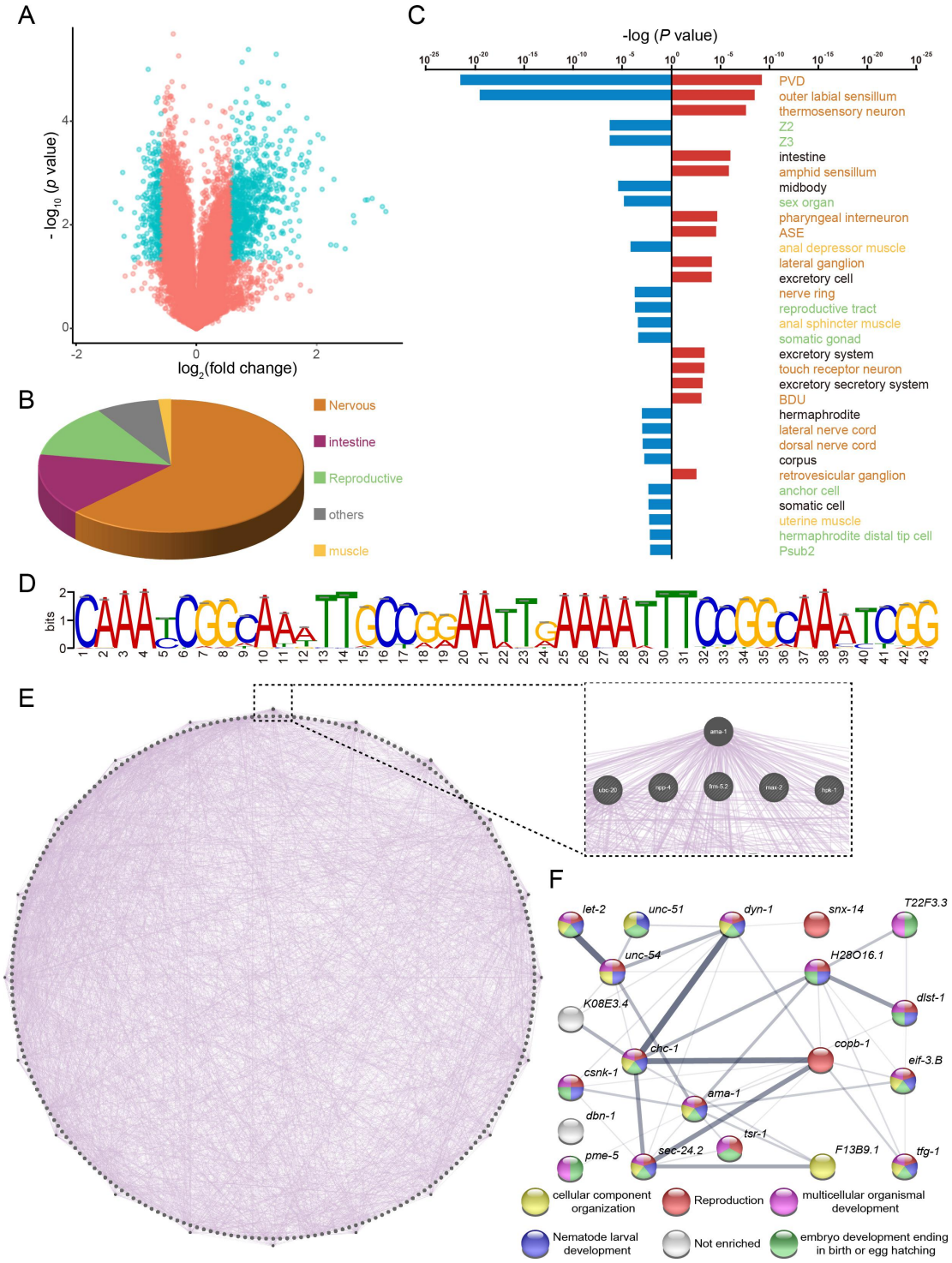
A
- log10 (p value)
log2(fold change)
B
Nervous
intestine
Reproductive
others
muscle
C
-log (P value)
PVD
outer labial sensillum
thermosensory neuron
Z2
Z3
intestine
amphid sensillum
midbody
sex organ
pharyngeal interneuron
ASE
anal depressor muscle
lateral ganglion
excretory cell
nerve ring
reproductive tract
anal sphincter muscle
somatic gonad
excretory system
touch receptor neuron
excretory secretory system
BDU
hermaphrodite
lateral nerve cord
dorsal nerve cord
corpus
retrovesicular ganglion
anchor cell
somatic cell
uterine muscle
hermaphrodite distal tip cell
Psub2
D
bits
E
F
let-2
unc-51
dyn-1
snx-14
T22F3.3
unc-54
H28O16.1
K08E3.4
dlst-1
chc-1
copb-1
csnk-1
eif-3.B
ama-1
dbn-1
tsr-1
pme-5
sec-24.2
F13B9.1
tfg-1
cellular component organization
Reproduction
multicellular organismal development
Nematode larval development
Not enriched
embryo development ending in birth or egg hatching

Figure 2

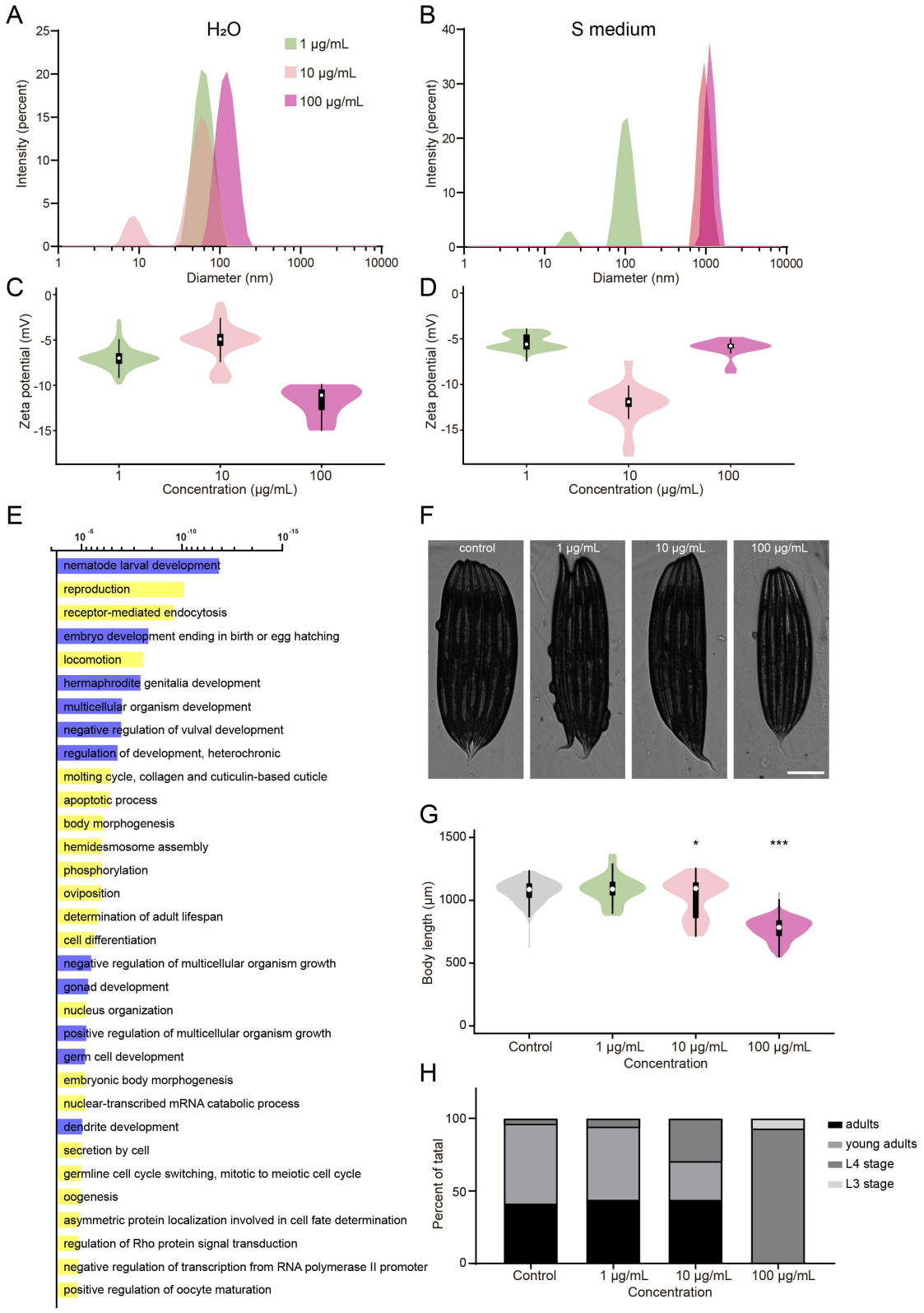
A
H₂O
1 µg/mL
10 µg/mL
100 µg/mL
Intensity (percent)
Diameter (nm)
B
S medium
Intensity (percent)
Diameter (nm)
C
Zeta potential (mV)
Concentration (µg/mL)
D
Zeta potential (mV)
Concentration (µg/mL)
E
nematode larval development
reproduction
receptor-mediated endocytosis
embryo development ending in birth or egg hatching
locomotion
hermaphrodite genitalia development
multicellular organism development
negative regulation of vulval development
regulation of development, heterochronic
molting cycle, collagen and cuticulin-based cuticle
apoptotic process
body morphogenesis
hemidesmosome assembly
phosphorylation
oviposition
determination of adult lifespan
cell differentiation
negative regulation of multicellular organism growth
gonad development
nucleus organization
positive regulation of multicellular organism growth
germ cell development
embryonic body morphogenesis
nuclear-transcribed mRNA catabolic process
dendrite development
secretion by cell
germline cell cycle switching, mitotic to meiotic cell cycle
oogenesis
asymmetric protein localization involved in cell fate determination
regulation of Rho protein signal transduction
negative regulation of transcription from RNA polymerase II promoter
positive regulation of oocyte maturation
F
control
1 µg/mL
10 µg/mL
100 µg/mL
G
Body length (µm)
Control
1 µg/mL
10 µg/mL
100 µg/mL
Concentration
H
Percent of tatal
adults
young adults
L4 stage
L3 stage
Control
1 µg/mL
10 µg/mL
100 µg/mL
Concentration

Figure 3

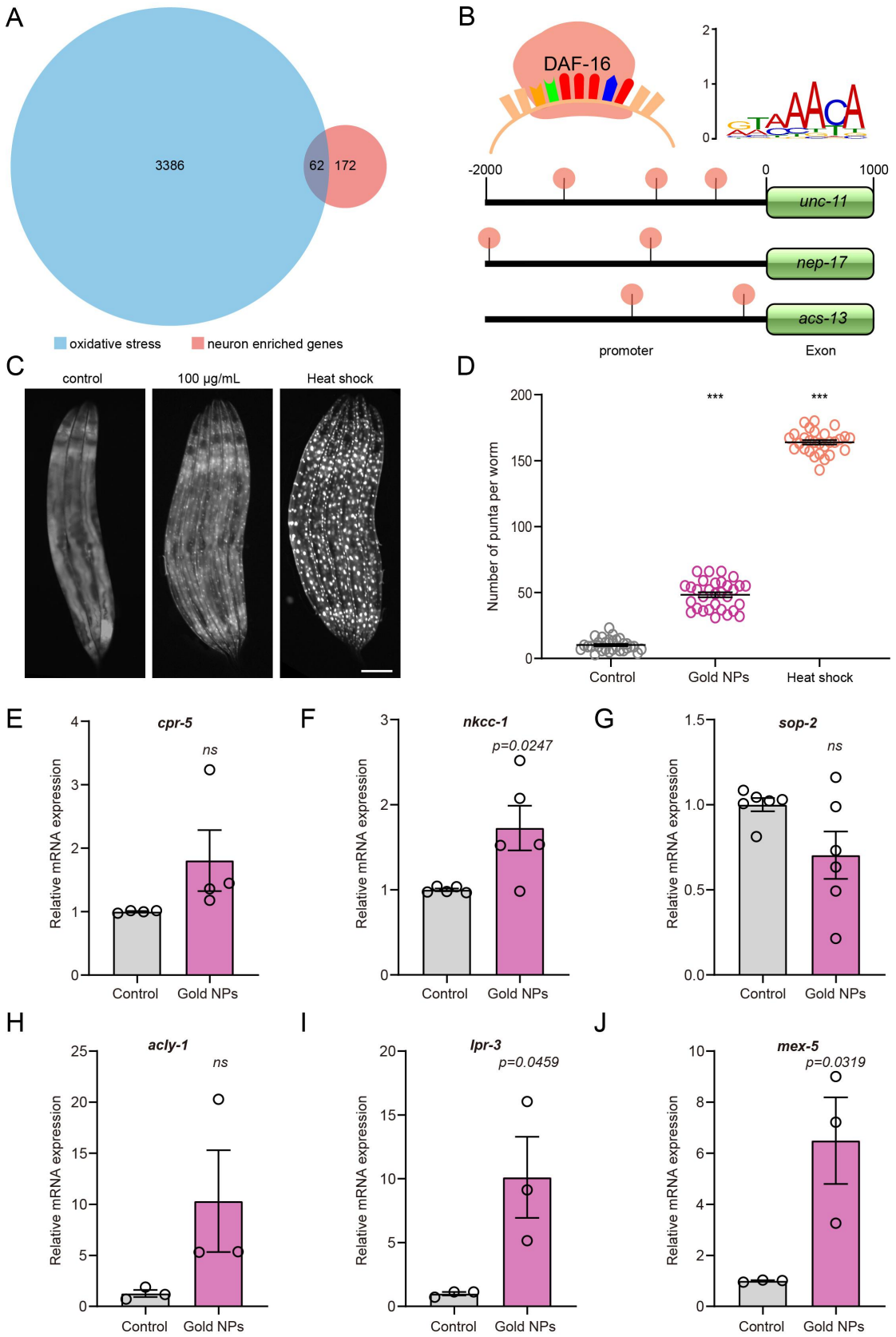
A
3386
62
172
oxidative stress
neuron enriched genes
B
DAF-16
-2000
0
1000
unc-11
nep-17
acs-13
promoter
Exon
C
control
100 µg/mL
Heat shock
D
Number of punta per worm
***
***
Control
Gold NPs
Heat shock
E
cpr-5
ns
F
nkcc-1
p=0.0247
G
sop-2
ns
H
acly-1
ns
I
lpr-3
p=0.0459
J
mex-5
p=0.0319
Relative mRNA expression
Control
Gold NPs

475 **Figure 4**

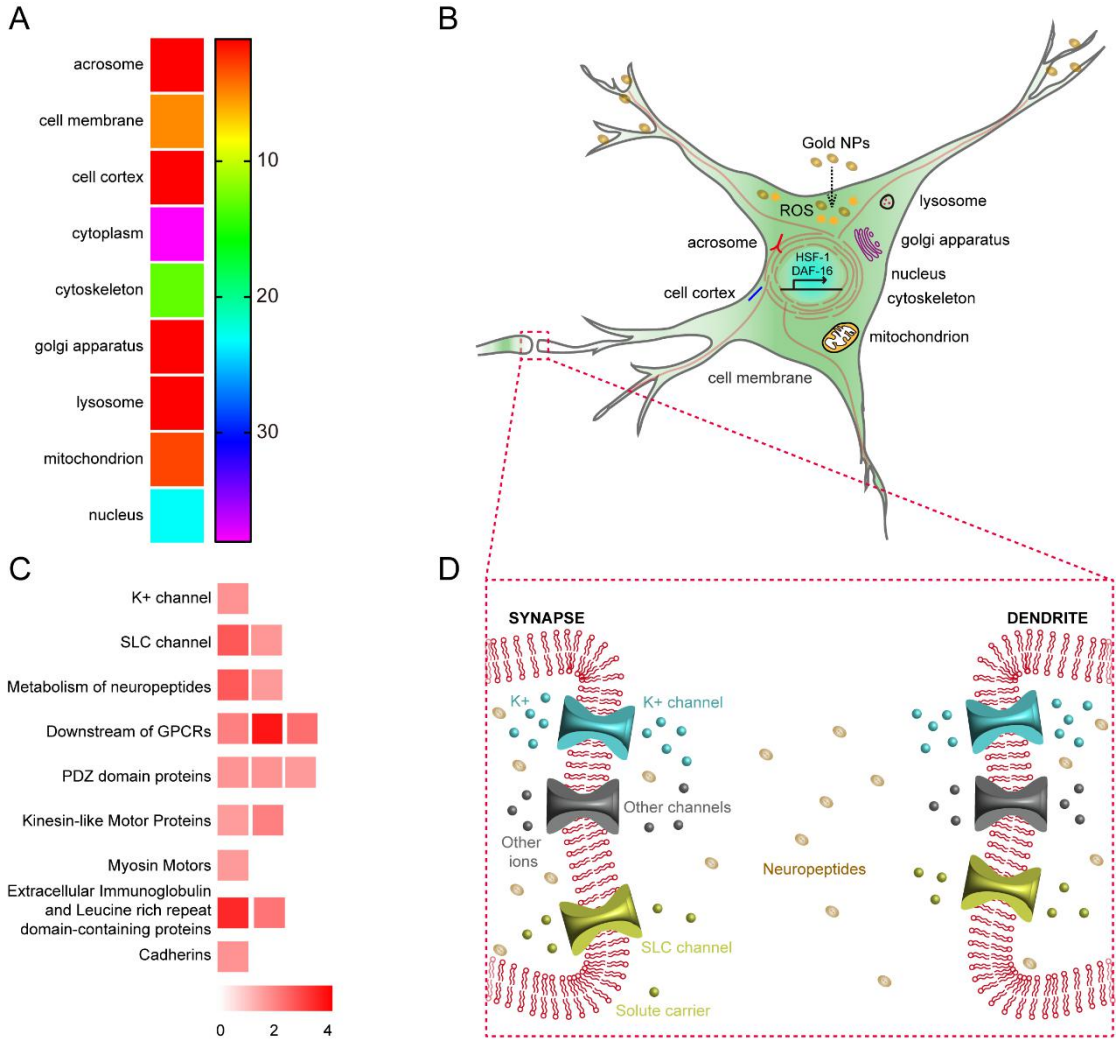

476